ELSEVIER

Biophysical Chemistry 54 (1995) 143–154

Biophysical Chemistry

Oxygen penetration and diffusion into myoglobin revealed by quenching of zincprotoporphyrin IX fluorescence

Jenny Carrero [a,*], David M. Jameson [b], Enrico Gratton [a]

[a] *Laboratory for Fluorescence Dynamics, Department of Physics, University of Illinois at Urbana-Champaign, Urbana, IL 61801-3080, USA*

[b] *Department of Biochemistry and Biophysics, University of Hawaii at Manoa, Honolulu, HI 96822, USA*

Received 27 June 1994, revised 21 November 1994; accepted 27 November 1994

Abstract

Oxygen quenching experiments were carried out on zincprotoporphyrin IX reconstituted myoglobin ($Mb^{Fe \rightarrow Zn}$) at different temperatures and two solvent viscosities. The data were fit to a dynamic model for quenching of fluorophores in protein interiors previously presented (Biophysical J., 45 (1984) 789–794). The parameters associated with the oxygen entry rate (k^+), exit rate (k^-), and migration rate (χ) in the protein were obtained at six temperatures and two viscosities (1 and 8 cp), along with the activation enthalpies associated with the above rates (k^+ and k^-). The partition coefficient (α) was calculated at each temperature along with the free energy, ΔG^0, associated with this partition. The rate parameters (k^+, k^-, χ) and the partition coefficient (α) have also been determined for the sample in 40% sucrose (8 cp), to evaluate the effect of bulk solvent viscosities on these values. The steady-state Stern–Volmer quenching plot was calculated using the rate parameters obtained from the analysis (of the dynamic model). Comparison of the Stern–Volmer points obtained using the dynamic model and those obtained experimentally showed excellent agreement.

Keywords: Oxygen penetration; Diffusion; Myoglobin; Quenching; Zincprotoporphyrin IX fluorescence

1. Introduction

Fluorescence quenching experiments using a variety of quenchers have contributed to our understanding of the dynamics of many proteins [1,2]. However, this information has been limited to fluorophore exposure to the quencher and an assessment of the electrostatic environment around the fluorophore. Oxygen quenching of tryptophan fluorescence in a number of globular proteins provided some of the early experimental evidence for the existence of conformational fluctuations in globular proteins [3]. These studies suggested that fluctuations in the protein must occur for the oxygen molecule to access the internally buried fluorophore. The exact time scale and mechanisms for the conformational fluctuations required for oxygen migration through the protein interior is still a matter of debate [1].

Vaughan and Weber [4] were the first to use oxygen quenching for fluorophores attached to proteins. They were able to carry out these studies at ambient oxygen concentration taking advantage of the long fluorescence lifetime (200 ns) of pyrene

* Corresponding author

SSDI 0301-4622(94)00133-2

butyric acid bound to bovine serum albumin (BSA). Using the Stern–Volmer equation they concluded that BSA was relatively impermeable to oxygen because the bimolecular quenching constant for the quenching of pyrene butyric acid bound to the protein was two orders of magnitude smaller than that for the fluorophore free in solution. Using a high-pressure spectroscopy cell, to increase the solution oxygen solubility, Lakowicz and Weber were able to quench the tryptophan fluorescence of many globular proteins, with lifetimes in the 2–6 ns range and concluded, again using the Stern–Volmer equation, that proteins are readily permeable to oxygen molecules [3]. The bimolecular quenching constants in this later study were found to be comparable to those obtained for N-acetyltryptophanamide in solution. The reason for these contradictory conclusions about oxygen permeation in proteins obtained using the same method of analysis was later addressed [5]. The explanation given was based on the inherent deficiency of the Stern–Volmer equation for the analysis of the quenching of internally buried fluorophores in a protein. A new model for the oxygen quenching, was proposed to specifically address this contradiction [5].

The experimental observation that led to the development of this model, a two process sequential model for the quenching of internally buried fluorophores, was first made by Coppey et al. [6]. Using frequency-domain fluorescence spectroscopy to study Hb^{desFe}, they observed that the introduction of oxygen into the system caused heterogeneity in the emission lifetimes, compared to single exponential decay in the absence of quencher. This observation, in fact, was anticipated by Lakowicz and Weber who also noted the differential behavior of the phase and modulation lifetimes in their systems as quenching occurred. The progressive heterogeneity of emission lifetimes with increasing oxygen concentrations was also observed by Jameson et al. [7] and in the present study. Heterogeneity in emission lifetimes has also been observed with quenchers other than oxygen at very high quencher concentration [8]. For fluorophores in solution, nonequilibrium statistical thermodynamics has been invoked to explain heterogeneity in emission lifetimes [9,10]. Molski and Keizer [9] proposed that this heterogeneity is based on the stationary nonequilibrium distribution of

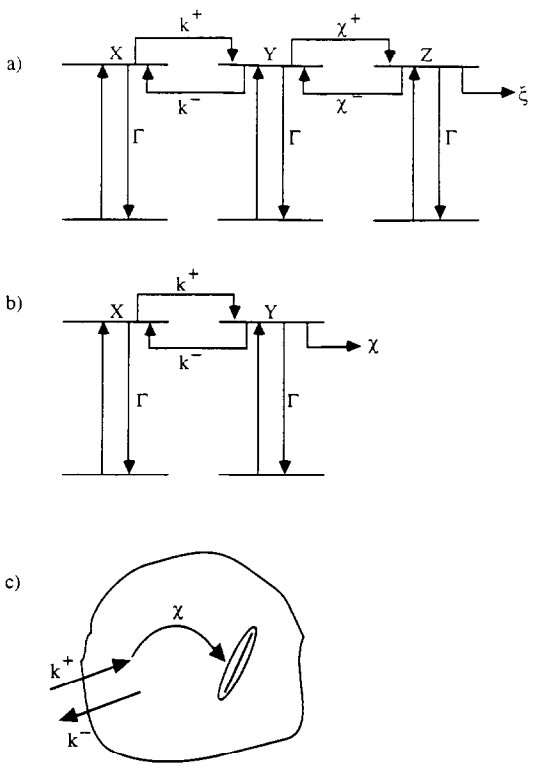

Fig. 1. (a) Full dynamic model; (b) simplified dynamic model; (c) representation of oxygen penetration and diffusion into the protein.

quencher molecules around an average fluorophore. They propose that time evolution of the radial distribution of the quencher concentration around the fluorophore causes the apparent bimolecular quenching constant to appear time dependent, which would result in lifetime heterogeneity. This mode is not relevant for myoglobin.

Gratton et al. [5] proposed a model for oxygen quenching of internally buried fluorophores in proteins that we will call the dynamic model for oxygen quenching, that can also account for the heterogeneity in emission lifetimes. The dynamic model will be summarized here, however, for a complete derivation, we refer the reader to the aforementioned work. In this model, the oxygen quenching of internally buried fluorophores is viewed as a sequential process that can be modeled as a three-state excited-state reaction (Fig. 1a). The three excited states of the model represents three predominant fluorophore cat-

egories in protein molecules, namely, fluorophores that remain unquenched, fluorophores that encounter quenchers originating external to the protein at the instant of excitation and fluorophores that encounter quenchers which are inside the protein at the instant of excitation (Fig. 1c)! This scheme essentially creates a sequential process which arises because of the interconversion of one molecular species into another during the excited state lifetime.

The relevant differential equations for the photophysical model shown in Fig. 1a are:

$$\frac{dX}{dt} - \Gamma_0 X + k^- Y \tag{1}$$

$$\frac{dY}{dt} = k^+[Q]X - \Gamma_1 Y + \chi^+ Z \tag{2}$$

$$\frac{dZ}{dt} = \chi Y - \Gamma_2 Z - \chi^- Z \tag{3}$$

$$\Gamma_0 = \Gamma + k^+[Q] \tag{4}$$

$$\Gamma_1 = \Gamma + \chi^+ + k^- \tag{5}$$

$$\Gamma_2 = \Gamma + \xi \tag{6}$$

where X is the concentration of protein molecules without quencher, Y is the concentration of protein molecules with quencher, Z is the concentration of protein molecules with quencher in the pocket, $k^+[Q]$ is the pseudo first-order entry rate into the protein, k^- is the exit rate from the protein, χ is the average migration rate throughout the protein. We assume that the ground-state and the excited-state equilibria are the same. The contribution of Z to the observed fluorescence intensity is negligible because the value for ξ is large with respect to χ^- and Γ. The Z state, then, is effectively a sink for the fluorescence and reduces the lifetime analysis to the simplified dynamic model (Fig. 1b). The two differential equations of the simplified model, which are coupled, are independent of Z and the solution is identical to that of an interconverting two-state system. The general solution of the coupled differential equations is:

$$X(t) = \alpha_{0x}\, e^{-m_0 t} \alpha_{1x}\, e^{-m_1 t} \tag{7}$$

$$Y(t) = \alpha_{0y}\, e^{-m_0 t} + \alpha_{1y}\, e^{-m_1 t} \tag{8}$$

where

$$m_{0,1} = \frac{(\Gamma_0 + \Gamma_1) \pm \sqrt{(\Gamma_0 - \Gamma_1)^2 + 4k^- k^+[Q]}}{2} \tag{9}$$

$$\begin{aligned}
\alpha_{0x} &= \frac{[X_0(\Gamma_0 - m_1) - k^- Y_0]}{m_0 - m_1}, \\
\alpha_{1x} &= \frac{[k^- Y_0 - X_0(\Gamma_0 - m_0)]}{m_0 - m_1} \\
\alpha_{0y} &= \frac{[Y_0(\Gamma_1 - m_1) - k^+[Q]X_0]}{m_0 - m_1}, \\
\alpha_{1y} &= \frac{[k^+[Q] - Y_0(\Gamma_1 - m_0)]}{m_0 - m_1}
\end{aligned} \tag{10}$$

Here X_0 and Y_0 are the population of the X and Y states at the instant of excitation.

The fluorescence intensity is proportional to the number of molecules in the excited state and the X and Y states have the same emission spectra. In this model, the fluorescence decay has two exponential components (m_0, m_1) that are not associated with the decay rate of the individual states, but are eigenvalues determined by k^+ [Q], k^-, Γ_0, Γ_1. A critical feature of this analysis is that the rate processes experimentally detectable are dependent on the decay rate of the excited state. This decay rate determines the relative concentration of the X and Y species and discriminates between the penetration and migration processes.

The inadequacy of the Stern–Volmer equation for the analysis of oxygen quenching in internally buried fluorophores should now be evident. The Stern–Volmer equation, $I_0/I = 1 + k^+ \tau_0[Q]$, was originally derived for a free fluorophore in solution [11]. The bimolecular quenching constant, k^+ represents the collision frequency between the fluorophore and the quencher. When the Stern–Volmer equation is applied to the analysis of internally buried fluorophores, the entry, exit, and migration rates for the oxygen quenching process are essentially lumped into this quenching constant. Longer lifetime probes require lower oxygen concentrations for quenching, so that the concentration of protein molecules with embedded oxygen at the time of excitation is negligible and, therefore, the quenching of the associated

fluorophores will have little contribution from the internal migration rate, if this rate is fast compared to the rate of quencher acquisition. Shorter lifetime probes require higher concentrations of dissolved oxygen to observe quenching, thereby providing an experimental situation, at the time of excitation, in which oxygen molecules are distributed both internal and external to the protein, permitting a sampling of all three rates of interest (k^+, k , χ). Therefore, the Stern–Volmer bimolecular quenching constant obtained with a short lifetime probe will essentially reduce to the migration rate, while the entry rate will be the predominant factor for a longer lifetime probe. Consequently, the Stern–Volmer bimolecular quenching constant will vary according to the magnitude of the unquenched lifetime, which, essentially creates the time window which determines which rate processes are emphasized and hence will not necessarily directly reflect the accessibility of the fluorophore to the quencher as was originally assumed.

The dynamic model for oxygen quenching was used by Jameson et al. [7] in a study on protoporphyrin IX reconstituted myoglobin to obtain k^+, k^-, χ, and the protein-to-solvent partition coefficient, α, at 20°C. The unquenched lifetime of protoporphyrin IX associated with apomyoglobin is about 16 ns. This relatively long lifetime emphasizes the entry and exit processes and hence cannot provide highly accurate values for the internal migration process. Also, in that study, the time resolution was not adequate to precisely assess the fast internal migration process. That study concluded that a much shorter lifetime probe would provide a better means to study the internal process which is more relevant to the dynamics of the protein matrix (Fig. 2). Therefore zincprotoporphyrin IX was chosen for the present study. The unquenched lifetime of this probe is about 2 ns, and hence affords greater accuracy in the determination of the rate of the internal process. This increased accuracy along with a temperature study allows us to determine the energy barrier associated with the different rate process. In fact, one of the goals of the study was to elucidate the thermodynamic parameters associated with the conformational fluctuations which result in oxygen entry.

In the present study on zincprotoporphyrin IX reconstituted myoglobin, we have performed oxygen quenching experiments at temperatures of 5, 10, 15, 20, 25, and 30°C while determining the lifetime using frequency domain methodologies and high modulation frequencies. The ability to carry out frequency-domain fluorescence measurements, with a broad range of frequencies, allows for the accurate measurement of the different rate processes that contribute to the quenching [12]. The Globals Unlimited software [13], which supports linked analysis of multiple data sets allowed fits directly to the simplified dynamic model. The activation energies for both viscosities were calculated with k^+ and k^- values obtained from the analysis at each temperature. The partition coefficient, α was calculated at each temperature along with the free energy, ΔG^0, associated with this partition. A steady-state Stern–Volmer plot was calculated from the dynamic model using the parameters obtained from the intensity decay analysis and estimating a value for the rate ξ of depopulation of the Z state as a function of collision with the quencher.

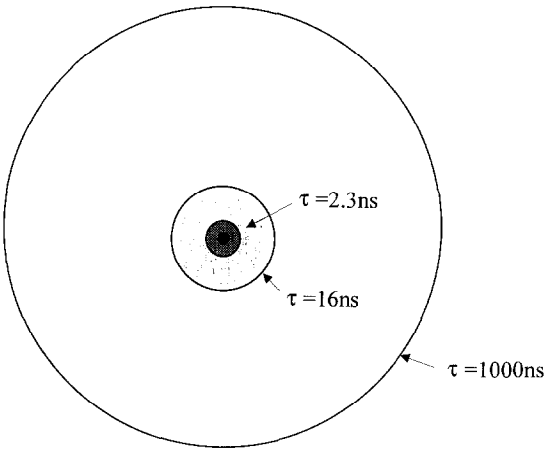

Fig. 2. Spheres of observation for lifetimes 1000, 16, and 2.3 ns compared to the radius of myoglobin (innermost sphere).

2. Materials and methods

Zincprotoporphyrin IX myoglobin was prepared from horse skeletal myoglobin (Sigma Chemical, St. Louis, MO) and zincprotoporphyrin IX (Porphyrin Products, Logan, UT). Heme extraction was performed using the acid–acetone method [14]. Por-

phyrin incorporation and purification of the final reconstituted protein was performed using previously published procedures [15]. These procedures removed excess porphyrin as well as any denatured protein. The incorporation of the porphyrin into the protein was examined using absorption and emission spectroscopy.

Quenching experiments were performed with a protein concentration of 5×10^{-6} M in 0.02 M phosphate buffer at pH 7.0 and 0.02 M phosphate buffer with 40% (w/w) sucrose. The gas pressure cell used in this study is similar to that described in previous oxygen quenching studies [3]. The pressure of the gas over the solution was determined with a Roylyn precision gauge (Roylyn Rueher Precision, Santa Ana, CA). The sample was continuously stirred with a magnetic stirrer. The sample was rapidly equilibrated with oxygen following a previously published method by Eftink and Ghiron [16], with a small modification. The tubing that introduced the gas into the sample was made approximately 20 cm long and coiled along the inside of the cell during measurements. This arrangement prevented any backflow of the sample through the teflon tubing into the stainless steel tubing, which occurred when the cell had to be reopened after a tight closure. The solubility of oxygen in water is: 1.93×10^{-3}, 1.74×10^{-3}, 1.54×10^{-3}, 1.41×10^{-3}, 1.27×10^{-3}, 1.15×10^{-3} M/atm at 5, 10, 15, 20, 25, and 30°C, respectively [17]. The solubilities of oxygen in 40% (w/w) sucrose are 1.34×10^{-3}, 1.21×10^{-3}, 1.07×10^{-3}, 0.98×10^{-3}, 0.88×10^{-3}, 0.80×10^{-3} M/atm at 5, 10, 15, 20, 25, 30°C. Sucrose (Sigma Chemical, St. Louis, MO) was recrystallized from an ethanol–water solution. The recrystallized sucrose, had no measurable emission under the conditions described for lifetime data acquisition, and therefore background subtraction was not required. The protein's visible absorption spectrum and the porphyrin emission spectrum were not altered by sucrose addition. Photobleaching of the zincprotoporphyrin IX did not occur at the light intensities utilized as evidenced by the lack of photoproduct after the experiment, which emits maximally near 670 nm [18].

Fluorescence lifetime measurements were performed using an ISS K2 multifrequency phase modulation fluorometer based on the instrument described by Gratton and Limkeman [19] and equipped with the digital electronic upgrading. The excitation source was an argon ion laser (Spectra Physics model 2045) tuned at 514 nm. Emission was observed through a 530 nm cuton filter (Hoya). The measured quantities, phase delay, and demodulation of the emission were made relative to the Rayleigh scatter of the sample. This scatter signal was observed through a 514 nm interference filter (Corion, Holliston, MA). The temperature was held constant with a temperature bath that was calibrated to obtain the desired temperature in the sample compartment. The exciting light was modulated at 12 frequencies between 30 and 150 MHz. Data were analyzed using the Globals Unlimited analysis program [13].

3. Results

The experimental data were in the form of phase and modulation values, for twelve modulation frequencies, for each temperature, oxygen pressure and solvent condition. For comparative purposes, the data were analyzed using three separate models the Stern–Volmer analysis, the double exponential decay, and the dynamic model. For the Stern–Volmer analysis, at each temperature, τ_0, the unquenched lifetime, and K_{SV}, the Stern–Volmer constant, were linked for all oxygen pressures (Table 1). In a similar fashion, for the double exponential decay analysis, τ_1 and τ_2 were linked for all oxygen pressures (Table 2). The effect of the pressure on the different data sets, in Table 2, is manifested in the different contribution of the fractional intensities associated with each of the two lifetime components (Fig. 3). Fig. 4 shows phase and modulation values as a function of frequency for the 25°C measurement.

Table 1
Stern–Volmer analysis

T (°C)	τ_0 (ns)	K_{SV} (M^{-1})	χ^2
30	2.29	0.92	20.6
25	2.32	0.83	23.6
20	2.24	0.75	23.0
15	2.33	0.64	26.1
10	2.33	0.53	23.1
5	2.35	0.49	28.7

Table 2
Double exponential decay analysis

T (°C)	τ_1 (ns)	τ_2 (ns)	χ^2
30	2.28	1.08	2.1
25	2.29	1.01	1.9
20	2.29	0.99	1.9
15	2.30	0.98	1.8
10	2.31	0.97	1.1
5	2.30	0.85	1.8

The phase and modulation curves shift to higher frequencies at higher oxygen pressures because of the shorter average lifetimes. The continuous line through the points shows the best fit to a double exponential decay. All of the temperature measurements can be fit to a double exponential decay with similar accuracy. A maximum of three parameters can be determined with a double exponential decay analysis at any given temperature and oxygen concentration. Data fit to the dynamic model were globally analyzed for four parameters: k^+, k^-, χ and Γ (Tables 3 and 4). By a separate analysis of the zero pressure measurement at each temperature, Γ is obtained. The complete determination of the other three parameters is possible by analyzing the data sets, taken as a function of oxygen pressure, using Eqs. (7) and (8) and the following considerations. The ratio of X over Y is proportional to $k^+[Q]/k^-$

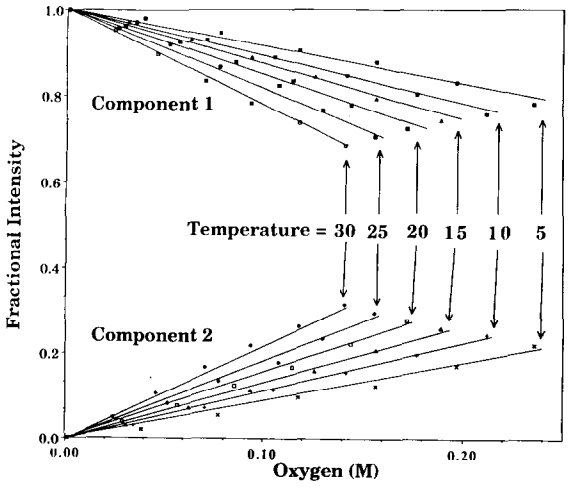

Fig. 3. Fractional intensities of components 1 and 2 from the double exponential analysis.

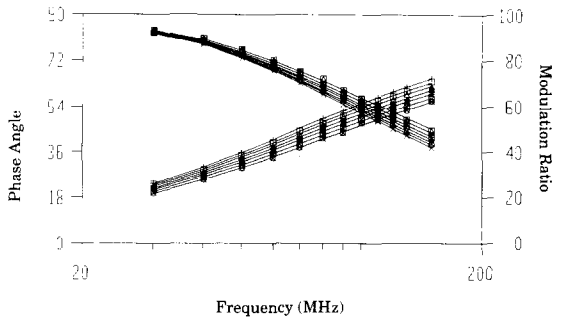

Fig. 4. Fit of double exponential model to the modulation, at 0 (×), 300 (○), 600 (×), 900 (◇) 1200 (×), 1500 (○), 1800 (×) psi and phase at 0 (+), 300 (□), 600 (△), 900 (☆), 1200 (+), 1500 (△), 1800 (□) psi at 25°C.

because X and Y have the same absorption coefficients and the emission spectra, and we assume that the equilibrium is not affected by excitation of the porphyrin. From the analysis, the migration rate (χ) was not significantly dependent on temperature or viscosity, therefore, after several attempts, the global analysis of all forty-two (seven pressures for six temperatures) data sets was performed with the rates linked throughout all the data sets. For all oxygen pressures at constant temperature, the radiative decay rate, Γ, was fixed to its zero oxygen pressure value and k^+ and k^- were linked along the different pressure data sets, but allowed to vary at different temperatures. The fit of the dynamic model is identical to that shown in Fig. 4. The errors associated with the dynamic model parameters were obtained by using the rigorous error estimation of the Globals Unlimited software [13].

The steady-state intensity for the fluorescence emission at all oxygen concentrations must be calcu-

Table 3
Zincprotoporphyrin IX myoglobin in 20 mM Na phosphate buffer

T (°C)	Γ_0 (10^9 s^{-1})	k^+ (10^9 s^{-1} M^{-1})	k^- (10^9 s^{-1})	χ (10^9 s^{-1})
30	0.436±0.003	0.55±0.05	0.14±0.02	2.6±0.2
25	0.435±0.003	0.44±0.05	0.12±0.02	2.6±0.2
20	0.434±0.003	0.37±0.05	0.11±0.02	2.6±0.2
15	0.434±0.003	0.31±0.05	0.10±0.02	2.6±0.2
10	0.432±0.003	0.26±0.03	0.09±0.02	2.6±0.2
5	0.432±0.003	0.20±0.03	0.08±0.01	2.6±0.2

Global $\chi^2 = 2.36$

lated by utilizing the full three-state model and is given by:

$$\langle F \rangle = \frac{\left[\alpha_{0x} + \alpha_{0y} + \left(\frac{k^+[Q]\alpha_{0y}}{\Gamma_2 - m_0}\right)\right]}{m_0} + \frac{\left[\alpha_{1x} + \alpha_{1y} + \left(\frac{k^+[Q]\alpha_{1y}}{\Gamma_2 - m_1}\right)\right]}{m_1} + \frac{\left[Z_0 - \left(\frac{k^+[Q]\alpha_{0y}}{\Gamma_2 - m_0}\right) - \left(\frac{k^+[Q]\alpha_{1y}}{\Gamma_2 - m_1}\right)\right]}{\Gamma_2} \quad (11)$$

This solution for the emission intensity is obtained by using Eqs. (7) and (8) and the following:

$$Z(t) = \left(\frac{k^+[Q]\alpha_{0y}}{\Gamma_2 - m_0}\right) e^{-m_0 t} + \left(\frac{k^+[Q]\alpha_{1y}}{\Gamma_2 - m_1}\right) e^{-m_1 t} + \left[Z_0 - \left(\frac{k^+[Q]\alpha_{0y}}{\Gamma_2 - m_0}\right) - \left(\frac{k^+[Q]\alpha_{1y}}{\Gamma_2 - m_1}\right)\right] e^{-\Gamma_2 t} \quad (12)$$

The value for ξ is too fast to be reliably measured even at the frequencies used in this study and hence can only be estimated. A very good agreement of the calculated steady-state intensity Stern–Volmer plot to the experimental steady-state intensity values was obtained by assuming a value of 10^{10} s^{-1} for ξ (Fig. 5).

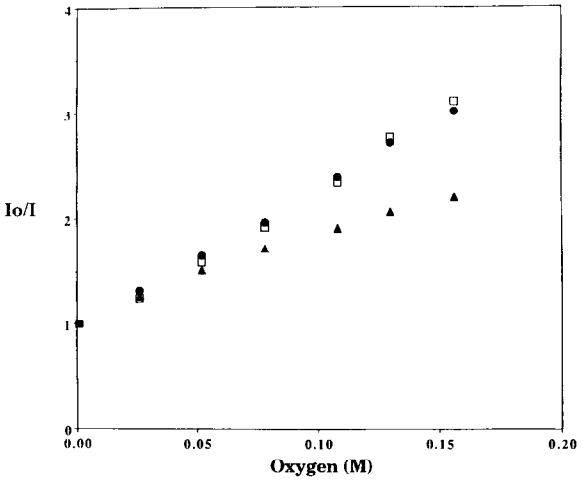

Fig. 5. Comparison of the calculated intensity using the simplified dynamic model (▲) and the full dynamic model (□) vs. experimental (●) Stern–Volmer at 25°C.

4. Discussion

Lifetime and steady-state data have been obtained for the oxygen quenching of zincprotoporphyrin IX reconstituted myoglobin in buffer and 40% sucrose. For the buffer case, the lifetime data was analyzed according to the three models discussed in the introduction, namely, the simple Stern–Volmer, double exponential decay and dynamic model and the results are evaluated. Using the dynamic model, rate constants associated with oxygen penetration and diffusion into myoglobin are obtained and used to understand the mechanism for the quenching of the porphyrin.

4.1. Simple quenching process

Comparison of the reduced chi-squares (goodness of fit), obtained with the simple Stern–Volmer analysis and that obtained with the double exponential decay, show that the double exponential decay provides a much better fit to the data (Tables 1 and 2). This finding unequivocally demonstrates that the quenching of an internally buried fluorophore by molecular oxygen is not adequately described by the simple Stern–Volmer equation. It also confirms that the fluorescence decay becomes heterogeneous with the introduction of oxygen into the system.

4.2. Two independent populations

The double exponential decay model represents the protein population as being composed of two fractions: one without quencher and one with quencher or two populations with different quenching rates. The absence of interconversion between these fractions during the lifetime of the fluorophore distinguishes this model from the dynamic model. In other words, these two models represent a parallel

process and a sequential process, respectively. Quenching experiments performed with a mixture of nitrogen and oxygen showed no difference in quenching behaviour from those performed with oxygen only (data not shown). Identity of quenching behaviour in the presence and absence of nitrogen can only occur if the interconversion rate between protein molecules with quencher and those without quencher takes place during the lifetime of the fluorophore. Hence the mixed gas experiment indicates that the parallel double exponential decay model is not appropriate. Moreover, the trend of the values as a function of oxygen concentration for the parameters obtained using the independent parallel process interpretation are inconsistent. In fact, inspection of the fractional intensity plots of Fig. 3 suggests that at a given oxygen concentration, the second component (the fraction of proteins containing oxygen at the time of excitation) is decreased at lower temperatures, and thus would lead to reduced quenching at lower temperatures. Instead, the trend of the lifetime values (Table 2) show that the second component is quenched better at lower temperatures. Both the mixed gas experiments and the results of the parallel double exponential analysis rule out a unique parallel quenching mechanism. Of course, if a large number of parallel quenching pathways are superimposed, then this more complex model can always fit the data.

4.3. Dynamic model analysis

From the mathematical point of view, the simplified dynamic model for the lifetime data is essentially a two-state model which yields a double exponential decay. As a consequence the global reduced chi-square using linked parameters for a fit using the two-state model can never be lower than that for a double exponential decay fit of the individual curves without constraints. However, it can be seen from the reduced chi-square that the dynamic model (Table 3) represents a much better fit to the data than the single exponential Stern–Volmer type (Table 1) of analysis and is not substantially worse than the average of the reduced chi-squares of the individual fits using double exponentials (Table 2). This agreement indicates that the simplified dynamic model may represent the mechanism for oxygen quenching of zincprotoporphyrin IX in horse skeletal myoglobin.

4.4. Activation energy analysis of entry and exit for the buffer

The activation energy for each of the rate processes was calculated using the Arrhenius equation (Fig. 6). The activation energy for k^+ is due to the activation energy barrier that must be overcome for the oxygen molecule, which originates in the solvent,

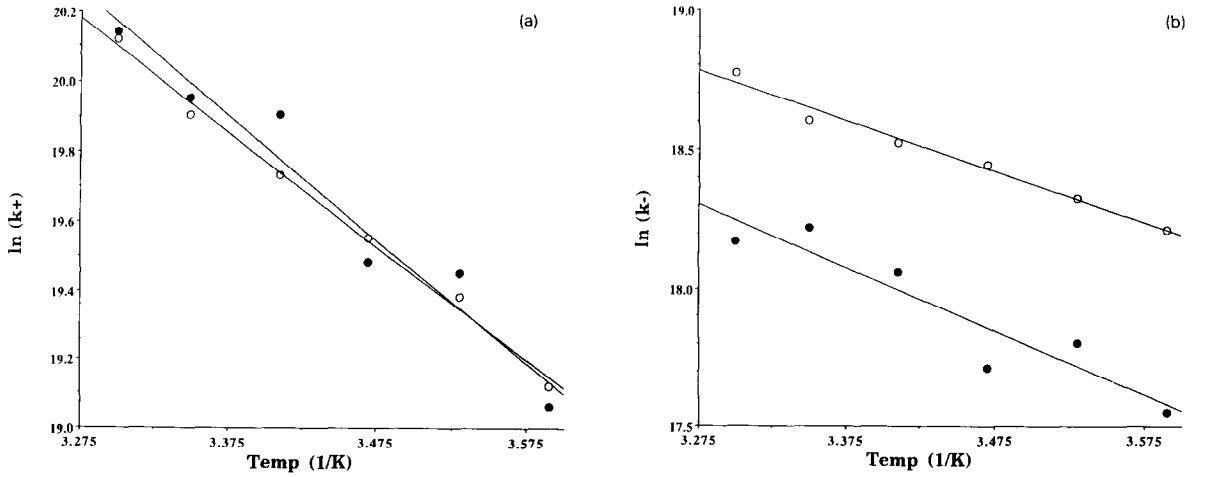

Fig. 6. (a) Arrhenius plots of k^+ for the buffer (○) and the 40% sucrose sample (●). (b) Arrhenius plots of k^- for the buffer (○) and the 40% sucrose sample (●).

to enter the protein. In this study, ΔH is is found to be 27 kJ/mole, in agreement with other quenching studies using zincprotoporphyrin IX reconstituted myoglobin [20]. Since free diffusion of oxygen in water has an activation energy of only 12.5 kJ/mole [3] this ΔH value signifies that the protein does, in fact, pose a barrier for oxygen entry. The rates and activation energies of entry obtained using flash photolysis [21] agree reasonably well with rates obtained using our dynamic model for fluorescence quenching of internally buried fluorophores, indicating that the two entry rates may measure the same processes. The entry rates obtained with the dynamic model also agree with bimolecular collision rates obtained by quenching of the triplet state and delayed fluorescence of zincprotoporphyrin IX [22,20] reconstituted myoglobin using a simple Stern–Volmer type of analysis. The agreement confirms that at the time of excitation, quenching of long-lived probes is accomplished by quenchers that originate external to the protein.

The value for enthalpy of activation for the exit process is 14.5 kJ/mole hence less than that for the entrance. The barrier for the entry and exit of oxygen is believed to originate at the protein–water interface. The oxygen molecule arriving to the protein migrates relatively quickly in the bulk water. The solvation shell at the protein–water interface determining the rate-limiting step for oxygen entry. The difference in activation enthalpies obtained for the oxygen entry and exit is due to the nature of the protein interior which is less polar than bulk water.

4.5. Analysis of the migration rate

The χ value is defined as the migration rate for the oxygen within the protein matrix to reach the excited porphyrin. Once the oxygen molecule is within a sphere of influence of the excited fluorophore [23], generally found to be the sum of the radii of the two molecules, it quenches the fluorescence. The reaction coordinate proposed by the Frauenfelder group [21] has two activation barriers in the native myoglobin that must be overcome for the binding of the oxygen to the heme from the solvent. The first barrier is proposed to be due to the entry of the oxygen into the protein. A fast, diffusion-like process occurs which brings the oxygen to the heme pocket. The second barrier is believed to be due to the iron in the heme and is not relevant for our quenching studies. In our study the migration rate is identified with the diffusion-like process and does not vary significantly with temperature. Fast processes that occur deep within the protein matrix have been shown to be weakly coupled to the solvent viscosity or temperature [24]. The quenching of internally buried tryptophans in the Lakowicz and Weber [3] experiments measured the migration through the protein which occurs in the nanosecond timescale. The migration rate obtain in this study is consistent with those results.

Table 4
Zincprotoporphyrin IX myoglobin in 20 mM Na phosphate buffer and 40% sucrose

T (°C)	Γ_0 (10^9 s^{-1})	k^+ (10^9 s^{-1} M^{-1})	k^- (10^9 s^{-1})	χ (10^9 s^{-1})
30	0.451±0.003	0.56±0.05	0.078±0.03	1.1±0.1
25	0.456±0.003	0.46±0.05	0.082±0.02	1.1±0.1
20	0.448±0.003	0.44±0.05	0.070±0.02	1.1±0.1
15	0.450±0.003	0.29±0.05	0.049±0.03	1.1±0.1
10	0.453±0.003	0.28±0.05	0.054±0.02	1.1±0.1
5	0.449±0.003	0.19±0.05	0.042±0.02	1.1±0.1

Global $\chi^2 = 2.01$

4.6. Oxygen partition coefficient

Determination of the entry and exit rates of the oxygen molecule allows for the calculation of the partition coefficient of oxygen in the protein as a function of temperature (Table 5). The protein is modeled after an immiscible layer in equilibrium with an aqueous layer. The ratios $k^+[Q]/k^-$ at each oxygen pressure are used to calculate the number of oxygen molecules per protein molecule [7] and then the molarity of oxygen in the protein by utilizing the volume of the protein and protein concentration yielding $\alpha = k^+/k^- V_p$, where k^+ and k^- have already been described and V_p is the molar volume of the protein (12 l/mole). The value of the partition coefficient for oxygen into the protein shows that apparently oxygen does not preferentially partition into the protein matrix and that lowering the temperature further reduces the solubility of oxygen in the protein. The reduced partition with temperature is a reasonable result since the solubility of oxygen in an

aqueous solution increases with the decrease in temperature [17]. The unexpected low partition of oxygen in the protein interior is probably a consequence of the volume in the protein which is excluded to the quencher. X-ray crystallography on many proteins has shown that 75% of the volume of the protein is occupied by atoms, assuming Van der Waals radii [25]. The resulting 25% free volume is possibly an overestimation since studies using continuous wave pressure perturbation show that the protein in solution has only 10–20% the compressibility of water [26] which has 48% free volume. This evaluation indicates that the fractional volume of the protein available for oxygen occupation can be as low as 5%. If the partition coefficient is corrected using a 5% accessible volume, solubilities comparable to those for oxygen in organic liquids are obtained.

The standard free energy, ΔG^0, for the partition were calculated using the following relation (Table 4):

$$\Delta G^0 = -RT \ln \alpha \quad (13)$$

where α is the partition coefficient already discussed, R is the universal gas constant and T is the temperature in Kelvins. A correction for the accessible volume would give a negative change in the standard Gibbs free energy that better represents the affinity of molecular oxygen for the less polar environment of the protein interior.

Table 5
Temperature dependence of the partition coefficient

T (°C)	α	ΔG (kJ/mole)
Buffer		
30	0.33±0.07	2.75±0.64
25	0.30±0.08	2.93±0.80
20	0.28±0.08	3.05±0.96
15	0.26±0.09	3.17±1.16
10	0.24±0.07	3.30±1.10
5	0.21±0.05	3.54±0.97
Buffer and 40% sucrose		
30	0.60±0.13	1.29±0.28
25	0.48±0.10	1.82±0.38
20	0.52±0.15	1.60±0.46
15	0.49±0.17	1.74±0.60
10	0.43±0.13	1.99±0.62
5	0.38±0.11	2.28±0.66

4.7. 40% sucrose experiments

The values for oxygen entry and the associated activation energy in 40% sucrose (29.6 kJ/mole) are not significantly different from those obtain for the buffer. The activation energy for the exit process is 19.2 kJ/mole in the sucrose which is 20% less than that found in the buffer case. The values for k^- are

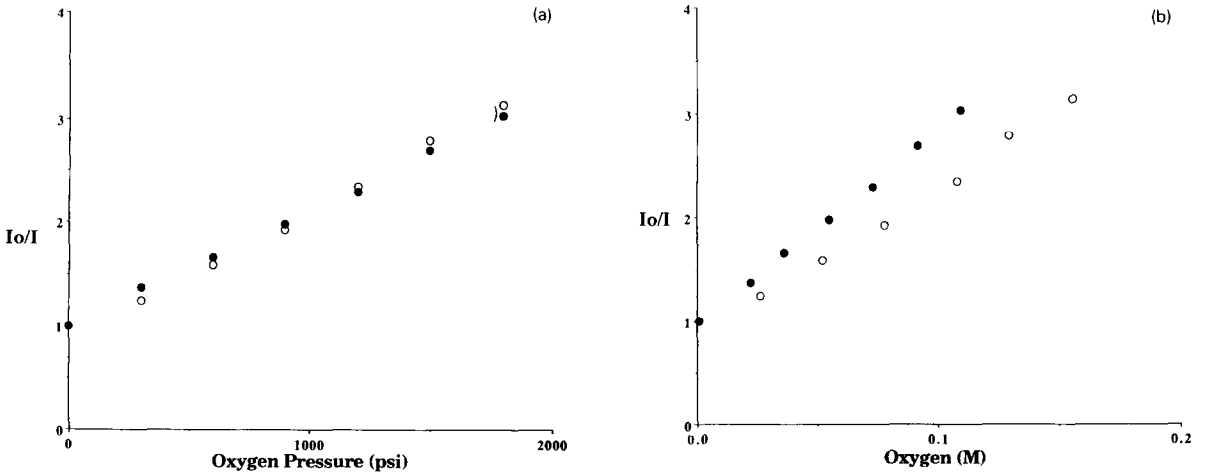

Fig. 7. (a) Intensity quenching of zincprotporphyrin IX myoglobin fluorescence in 40% sucrose (●) and buffer (○) plotted vs. oxygen pressure. (b) Intensity quenching of zincprotporphyrin IX myoglobin fluorescence in 40% sucrose (●) and buffer (○) plotted vs. oxygen concentration.

also less than those for the buffer case (Tables 3 and 5).

To understand the effect of the 40% sucrose on k^+ and k^- and the activation energies, recall that the entry rate is probably affected primarily by the solvation shell. Sucrose is thought to be excluded from the solvation shell of the protein [27] and will probably not have a significant affect on this shell and therefore the entry rate or the barrier height. The decrease in the exit rate is expected because the oxygen molecule originates in the protein and must transfer to the solvent where the solubility is decreased. In both solvents, the buffer alone and the buffer with sucrose, and at all pressures the oxygen in the protein is in equilibrium with the external oxygen pressure (Fig. 7a). The solvent has no effect on the partition of oxygen established between the protein phase and the gas phase hence the activation energy remains the same in both solvents (Fig. 6). In fact plotting the Stern–Volmer intensity quenching for the solvent in terms of the concentration of oxygen in the solvent will erroneously depict increased quenching, and therefore oxygen solubility in the protein, in the sucrose solvent (Fig. 7b). The 32% decrease of oxygen solubility at 20°C in the sucrose results in an increase in free energy for the oxygen in the sucrose as compared to the oxygen in the buffer, which accounts for the relative greater partitioning of oxygen in the protein with respect to this solvent and the increase in the activation barrier height for oxygen exit (Fig. 6b).

4.8. Calculation of the steady–state Stern–Volmer plot

The lifetime data were found to be accurately represented by the simplified dynamic model. However, the steady-state Stern–Volmer plot calculated using the parameters from the simplified dynamic model deviates significantly from the traditional experimental Stern–Volmer plot (Fig. 5). The calculation of the emission intensities requires the use of all the parameters described in the three-state form of the dynamic model including the rate ξ. This parameter represents the rate of excited state depopulation. A very fast process appears as a 'quasi-static' quenching term and significantly affects the steady-state intensity but has very little effect on the intensity decay expected at very short times. The modulation frequencies used in this study were not high enough to permit accurate determination of this very fast process. A value for ξ of about 10^{10} s^{-1} is assumed in order to calculate the intensities for the Stern–Volmer and comparison with the experimental steady-state Stern–Volmer shows excellent agreement (Fig. 5). The feasability of the order of magnitude of the assumed value for ξ was examined by estimating the rate of diffusion of the oxygen molecule during the 'collisional time'. The calculated distance traveled by the oxygen molecule during the period, ξ, using the diffusion constant in water (2×10^{-5} cm^2/s), is 4.5 Å. Assuming that the diffusional rate of oxygen can be at least one order of magnitude lower in the protein than in water (2×10^{-6} cm^2/s), the distance traveled would be 1.4 Å. This length is essentially that of an oxygen molecule. Comparison of the assumed ξ rate with the geminate recombination rate attributed to recombination of the ligand with the heme from a close contact position shows very good agreement [28]. We conclude that the ξ value assumed for the fit is reasonable and that it can represent quenching from the pocket.

4.9. Comparison with previous studies

Finally, comparison of the rates obtained with zincprotoporphyrin IX myoglobin with those obtained with protopophyrin IX [12] shows that the values for the entry and the exit rate agree to within 2%. This agreement is significant because it demonstrates that the nature of the porphyrin did not affect the dynamics associated with oxygen entry or exit. Zincprotoporphyrin IX reconstituted myoglobin has previously been shown to have different antibody binding properties than protoporphyrin IX reconstituted myoglobin [29]. We conclude that the structural changes that elicit different antibodies do not play a significant role in the dynamics of oxygen entry or exit.

The χ values for this study differ by an order of magnitude from the previous study. There are two major differences between the two studies that, taken in conjunction, may contribute to this difference in this value. The former study used a longer lifetime probe ($\tau_0 = 16$ ns) and the instrumentation was, at

that time, limited to 36 MHz for the highest light modulation frequency. The present study used a shorter lifetime probe and frequencies up to 150 MHz, to enhance detection of faster processes, and is therefore more accurate than the former study and the difference may just be due to greater accuracy. However, it is also possible that the structural differences that were observed by Andres and Atassi [29] are manifested primarily in the migration rate of oxygen to the porphyrin. In conclusion, the dynamic model has been shown to fit reasonably well to the quenching data, including the correct prediction of the steady-state intensity at all oxygen concentrations.

Acknowledgments

The experiments and the analysis of the data produced were performed jointly at the Laboratory for Fluorescence Dynamics (LFD) at the University of Illinois at Urban-Champaign (UIUC) and at the University of Hawaii at Manoa. The LFD is supported jointly by the Division of Research Resources of the National Institutes of Health grant PHS-P41-RR03155 (JC, EG), UIUC and National Science Foundation grant DMB 9005195 (DMJ).

References

[1] M. Eftink, in J.R. Lakowicz (Editor), Topics in Fluorescence Spectroscopy, Vol. 2, Plenum Press, New York (1991).
[2] S. Papp and J.M. Vanderkooi, Photochem. Photobiol., 49 (1989) 775–784.
[3] J.R. Lakowicz and G. Weber, Biochemistry, 12 (1973) 4171–4179
[4] W.M. Vaughan and G. Weber, Biochemistry, 9 (1970) 464–473.
[5] E. Gratton, D.M. Jameson, G. Weber and B. Alpert, Biophysical J., 45 (1984) 789–794.
[6] M. Coppey, D.M. Jameson and B. Alpert, FEBS Lett. 126 (1981) 191–194.
[7] D.M. Jameson, E. Gratton, G. Weber and B. Alpert, Biophysical J., 45 (1984) 795–803.
[8] J.R. Lakowicz, M.L. Johnson, I. Gryczynski, N. Joshi and J. Laczko, J. Phys. Chem., 91 (1987) 3277–3285.
[9] A. Molski and J. Keizer, J. Phys. Chem., 97 (1993) 8707–8712.
[10] H.X. Zhou and A. Szabo, J. Chem. Phys. 92 (1990) 3874–3880.
[11] O. Stern and M. Volmer, Z. Phys., 20 (1989) 183–189.
[12] D.M. Jameson, E. Gratton and R.D. Hall, Appl. Spectrosc. Rev., 20 (1984) 55–106.
[13] J.M. Beechem, W.W. Mantulin and E. Gratton, Globals Unlimited Software Program, University of Illinois, Urbana, IL (1988).
[14] F. Ascoli, M. Fanelli and E. Atonini, Methods Enzymol., 76 (1981) 72–90.
[15] H. Zemel and B.M. Hoffman, J. Am. Chem. Soc., 103 (1981) 1192–1201.
[16] M. Eftink and C.A. Ghiron, Photochem. Photobiol., 50 (1989) 425–427.
[17] E.W. Washburn (Editor), International Critical Tables, Vol. 3, 1st ed McGraw-Hill, New York, 1928, pp. 257 and 272.
[18] P. Valat, G.D. Reinhart and D.M. Jameson, Photochem. Photobiol. 47 (1988) 787–790.
[19] E. Gratton and M. Limkeman, Biophysical J., 44 (1983) 315–324.
[20] N. Barboy and J. Feitelson, Biochemistry, 28 (1989) 5450–5456.
[21] P.J. Steinbach, A. Ansari, J. Berendzen, D. Braunstein, K. Chu, B.R. Cowen, D. Ehrenstein, H. Frauenfelder, J.B. Johnson, D.C. Lamb, S. Luck, J.R. Mourant, G.U. Neinhaus, P. Ormos, R. Philipp, A. Xie and R.D. Young, Biochemistry, 30 (1991) 3988–4001.
[22] B. Alpert and L. Lindqvist, Science, 187 (1975) 836–837.
[23] I.M. Frank and Vavilov, Z. Phys. 69 (1931) 100–107.
[24] M. Settles, F. Post, D. Muller, A. Schulte and W. Doster, Biophys. Chem., 43 (1992), 107–116.
[25] F.M. Richards, Ann. Rev. Biophys. Bioeng., 6 (1977) 151.
[26] B. Gavish, E. Gratton and C.J. Hardy, Proc. Natl. Acad. Sci. USA, 80 (1983) 750–754.
[27] S.N. Timasheff, J.C. Lee, E.P. Pittz and N. Tweedy, J. Colloid Interface Sci., 55 (1976) 658–664.
[28] K.A. Jongeward, D. Magde, D.J. Taube, J.C. Marsters, T.G. Traylor and V.S. Sharma, J. Am. Chem. Soc., 110 (1988) 380–387.
[29] S.F. Andres and M.Z. Atassi, Biochemistry, 9 (1970) 2268–2275.